Hindawi Publishing Corporation
Shock and Vibration
Volume 2016, Article ID 2741748, 10 pages
http://dx.doi.org/10.1155/2016/2741748

Research Article

Research on Thermal-Field and Sound-Field Coupling Properties of Different Grid Forms

Enlai Zhang, Liang Hou, Huikun Cai, Chao Shen, and Yaxiang Zhang

Department of Mechanical and Electrical Engineering, Xiamen University, Xiamen 361005, China

Correspondence should be addressed to Liang Hou; hliang@xmu.edu.cn

Received 15 July 2015; Accepted 15 October 2015

Academic Editor: Jussi Sopanen

The inlet grid and exhaust grid are widely used in engineering machinery products. The process that airflow goes through grids is a complex turbulent flow and directly related to the heat dispersion and aerodynamic noise. The theoretical analysis result shows that the jet noise generated by airflow has a connection with the grid structure form, fluid flowing situation, and heat conduction. In addition, the influences of different grid structure forms (included the round hole, long hole, and square hole) and porosity on the heat dissipation and aerodynamic noise were analyzed and presented based on the verified computational fluid dynamics (CFD) model. Results show that the heat dispersion and aerodynamic noise of the round hole are most effective under the same porosity; as the porosity increases, the disturbance degree decreases and the noise reduction effect gets better. Finally, the research result provides the scientific basis for improving grid structure and achieving energy saving and noise reduction.

1. Introduction

(1) Research Background and Methods. In today's market, it has become the key points of competition and the threshold of import and export trade to improve the product performance, energy saving, and noise reduction of engineering machinery [1, 2]. And the heat dispersion of engine compartment has effects on its operational reliability and service life. Also, the radiation noise has a direct link to the economical efficiency and market adaptation of mechanical products. In the practical application, the heat dispersion of the engine compartment is mainly realized by the forced-convection heat transfer through a cooling fan. When air enters the engine compartment system through the inlet grid, it takes away the superficial heat of a radiator and other structures. In the end, the heat is spread out of the system from the exhaust grid. As sound velocity increases when the temperature of medium increases, sound wave propagates along the direction of the largest temperature gradient in the temperature field [3]. Based on those facts mentioned above, the structure form and porosity of the grid have a direct relation with the heat dispersion and aerodynamic noise of the whole engine compartment.

When air goes through grids, the generated noise mainly resulted from instable airflow, that is, fluid mechanics factors. The process of air flow is complicated and there is constant heat exchange with surrounding medium when making the jet noise. There are mainly two methods to study fluid noise and heat exchange: numerical simulation and experimental research [4–7]. For example, Khaled et al. took use of three-dimensional numerical simulation and experimental research to explore the influence of inflow grid surface and ground angle on the cooling system performance under different vehicle speeds [8]. However, there are some disadvantages for the method of experimental research such as long design cycle, large cost, and time consumption. With the rapid development of information technology, computational fluid dynamics (CFD) method provides a new approach for solving the above problems [9–12]. In addition, many scholars have verified the feasibility of CFD in the numerical simulation of airflow field. For instance, Aguilar et al. presented a numerical study of a double pan window and analyzed the room temperature and the incident solar radiation by CFD, and the research results achieved the purpose of saving energy [13]. Cui et al. adopted Eulerian-Lagrangian CFD model to investigate the performance of the evaporative air cooler under a variety of conditions and validated the model

by comparing the temperature distributions and outlet air conditions against experimental data [14]. Tolias et al. used CFD modeling techniques to simulate homogenous deflagration based on the turbulent flame speed concept, and the agreement between experimental and computational results was satisfactory in both empty and no-empty tunnel cases [15].

Therefore, based on the essential research field and effective method, this paper is focused on coupled issue of thermal field and sound field under different grid forms as well as different porosities and presents the numerical simulation analysis by the CFD method, which has not been reported so far. The calculation results are going to provide theoretical foundation on saving energy and reducing noise for the whole machine.

(2) Description of the Paper Organization. The paper is organized as follows. Section 2 introduces the theoretical analysis of airflow passing through grids to take into account the influence of the grid structure form, fluid flowing situation, and heat conduction on the jet noise. Section 3 presents the numerical calculation models of three grid forms established by CFD method. Section 4 shows the experiment to verify that the built CFD model is accurate. Section 5 collects the coupling results of the thermal field and sound field, and an analysis of the relations between the flow field, total heat release (THR) and average sound pressure level (ASPL), and porosity and the fluid velocity is done. Finally, conclusions are drawn in Section 6.

2. Theoretical Analysis

In this paper, the effect of the inlet grid and exhaust grid in the engine compartment of a certain engineering machinery product on the coupling of thermal field and sound field was taken as the research target. The distribution and physical models of the inlet grid and exhaust grid are shown in Figures 1, 2, and 3.

The airflow sprays out through grids at a relative high speed and makes noise, which is referred to as jet noise [16, 17]. Even though the process of generating jet noise is complex, its mechanism and source characteristics can still be analyzed with axisymmetric free jet [18].

Figure 4 shows the structure of axisymmetric free jet with the grid hole diameter to be D. When airflow sprays into still air through the grid hole, the full-developed turbulence is generally divided into three zones: mixed zone, transition zone, and full-developed zone [19, 20]. In the mixed zone, the airflow is a nearly full turbulent flow and the airflow movement in the taper area surrounded with mixed zone maintains laminar flow. Thus, this area is called potential core. After the mixed zone, it is the transition zone full of turbulence, but the average velocity of the jet in this zone gradually decays. After that, it comes to the full-developed zone, in which the airflow is a kind of the flow maintained by itself.

The jet intensity, which is defined as the ratio of the axial velocity fluctuation to the nozzle velocity, is relative to the velocity gradient. Through the noise test, it has been proved

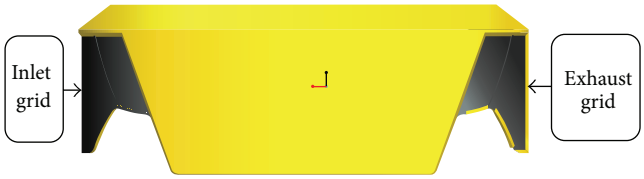

Figure 1: Distributions of the inlet grid and exhaust grid in an engine compartment.

Figure 2: Actual inlet grids.

Figure 3: Actual exhaust grids.

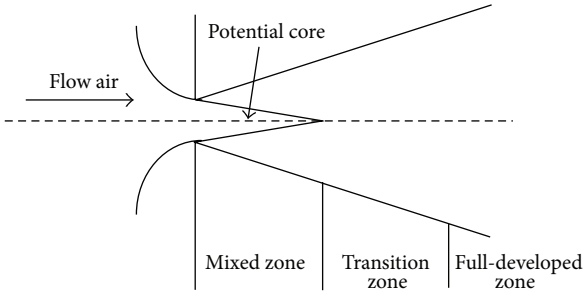

Figure 4: Analysis model of airflow going through the grid.

that jet noise is mostly generated by the turbulence in the mixed zone and the transition zone, which is linked to the turbulence intensity.

The sound field of air jet follows the wave equation of active acoustic field [17]. In 1969, Ffowcs Williams and Hawkings put forward FW-H equation to simulate the generation and propagation of sound [21–23]. Through the integral on the time domain, the equation can indicate some basic solution distributions such as pure monopole, dipole, and quadrupole. It is considered to be the accurate recombination of the continuum equation and the Navier-Stokes equation [24, 25].

And the continuum equation can be expressed as

$$\frac{\partial \rho}{\partial t} + \frac{\partial \rho v_i}{\partial x_i} = 0. \quad (1)$$

The Navier-Stokes equation is described as

$$\rho \frac{\partial v_i}{\partial t} + \rho v_j \frac{\partial v_i}{\partial x_j} = \frac{\partial p_{ij}}{\partial x_j}. \quad (2)$$

Suppose that the movement control surface is penetrable and discontinuous, and all flow variables are the generalized function. Thus, the FW-H equation can be deduced according to the property of the generalized function, which is given by the following equation [26]:

$$\frac{\partial^2 \rho}{\partial t^2} - c_0^2 \nabla^2 \rho = \frac{\partial Q(x,t)}{\partial t} - \frac{\partial F_i(x,t)}{\partial x_i} + \frac{\partial^2 T_{ij}}{\partial x_i x_j}, \quad (3)$$

where ∇ is Laplacian operator; c_0 is the propagation velocity of sound wave; Q is the increased fluid quality per second and unit volume at the moment of t and the position of X; F is the force per unit volume; T_{ij} is the stress tensor of Lighthill. The three terms on the right of the equation stand for the sound source of pure monopole, dipole, and quadrupole, respectively. It is known that the sound source of dipole is related to the form and structure of the object. Also, the sound source of quadrupole is turbulent sound source and relates to fluid velocity.

The stress tensor T_{ij} can be expressed as

$$T_{ij} = \rho u_i u_j + p_{ij} - c_0^2 \rho \delta_{ij} = \rho u_i u_j + \left(p - c_0^2 \rho\right) \delta_{ij} - \tau_{ij}, \quad (4)$$

where u stands for instantaneous velocity; $\rho u_i u_j$ is the convection momentum; $(p - c_0^2 \rho)\delta_{ij}$ is the heat conduction; τ_{ij} is the viscous stress.

It can be seen that the radiation of aerodynamic noise is mainly influenced by the structure form of the grid and fluid flowing situation, which is furthermore related to fluid heat conduction.

3. CFD Model

As airflow goes through the grid is a process of turbulence, its flow process should be described by turbulence equation. There is no exact solution for the turbulence equation; thus the main research method is numerical simulation. This paper adopted Fluent, a simulation software of computational fluid mechanics, to analyze the distribution of flow field, thermal field, and sound field under different grid forms and different porosities. The result of numerical simulation is of great significance for improving engine compartment's performance on saving energy and reducing noise.

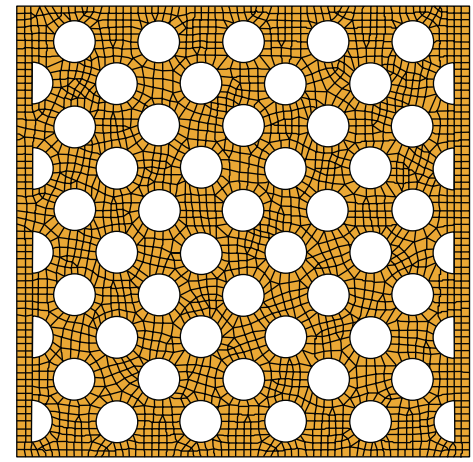

Figure 5: Round hole grids.

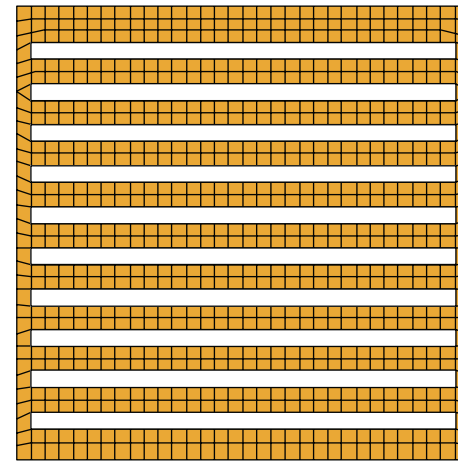

Figure 6: Long hole grids.

3.1. Establishment of Finite Element Model. In practice, there are as many as thousands of holes in the inlet grid and exhaust grid, seen in Figures 2 and 3. The diameter of hole is 6 mm and the distance of holes is 12 mm. It is extremely difficult to establish 3D model and mesh generation due to the large number of holes and the small size of hole. In order to research the coupling properties of thermal field and sound field in engine compartment under different grid structures, three common types of grid were adopted: round hole, long hole, and square hole with the same porosity which is defined as the ratio of opening area to grid area. In addition, the 3D models and finite element models of the three grid forms were separately established by Pro/E software and HyperMesh software (Figures 5, 6, and 7).

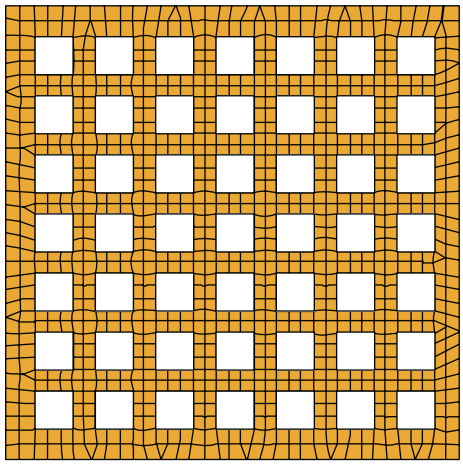

Figure 7: Square hole grids.

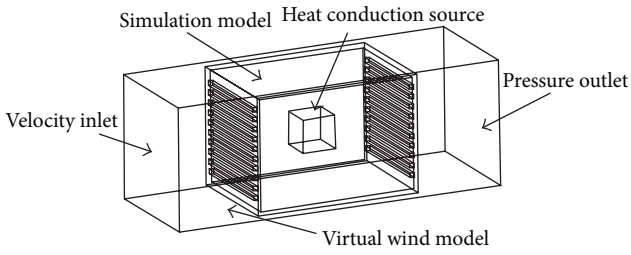

Figure 8: CFD model for numerical simulation.

When air enters the engine compartment through the inlet grid, it takes away heat from the radiator and other structure surfaces. As the internal system of the engine compartment is extremely complicated, the internal heat source systems are simplified to be a heat conduction source, and then three different types of simulation model and virtual wind tunnel were established, shown in Figure 8. In the model, the size of simulation model is 68 mm × 68 mm × 100 mm; thus according to the actual size of the round hole, porosity can be figured out $p = n\pi d^2/(4D^2) = 0.345$ (where n is the number of holes; d is the diameter of the round hole; D is the side length of the simulation model), and the size of virtual wind model is 76 mm × 76 mm × 200 mm.

3.2. Boundary Condition. The kind of the inlet boundary and outlet boundary in virtual wind model were velocity-inlet and pressure-outlet, respectively. In addition, the material kind of fluid and wall were air and steel, respectively. And the wall was simulated using the nonslip boundary condition. The parameters of air and steel were set, as shown in Table 1.

The shape of heat source is determined to be a cube with the side length of 20 mm. Based on the parameters provided by the manufacturer, the THR and the option value of sources in Fluent software are set to be 8×10^3 W and $1e + 09$ W/m^3, respectively.

In practice, as the airflow through grid is a type of bend flow after touching the system structures, the effect of wall needs to be taken into consideration. According to the character of bend flow, the relatively mature turbulence model *RNG k-e* thus was applied and the algorithm of SIMPLE was adopted to get the solution [27]. Furthermore, the difference scheme of momentum, turbulent kinetic energy, turbulent dissipation rate, and energy equation were determined to be first-order upwind difference scheme and the calculation values of turbulence intensity and hydraulic diameter were set.

Table 1: Parameters of air and steel.

Parameters	Air	Steel
Density (kg/m^3)	1.225	8030
Specific heat (j/kg-k)	1006.43	502.48
Thermal conductivity (w/m-k)	0.5	63

Table 2: Relation between the fluid velocity and the turbulence intensity.

Fluid velocity (m/s)	11.6	12.6	13.6	14.6	15.6	16.6
Turbulence intensity (%)	4.13	4.09	4.049	4.012	3.979	3.948

Turbulence intensity is defined as the ratio of velocity fluctuation's root-mean-square to the average velocity. As a significant indicator of turbulence flow characteristic, it reflects the fluctuation intensity of fluid. It can be calculated by the following formula:

$$I = 0.16\,\mathrm{Re}^{-1/8}, \tag{5}$$

where Re is Reynolds number, $\mathrm{Re} = \rho v L/\mu$, and it represents the dimensionless number of fluid situation; ρ and μ are the density of fluid and the coefficient of kinetic viscosity; v and L are the characteristic velocity and characteristic length of flow field.

Hydraulic diameter is the characteristic length used to calculate the Reynolds number of noncircular tube flow. Its computational formula is described as

$$d_H = \frac{4A}{S}, \tag{6}$$

where S is the wetted perimeter through the turbulence; A is the area through turbulence surface; hydraulic diameter is the feature size.

According to the actual fluid velocity near the engine compartment, six different fluid velocities were selected in simulation and they are 11.6 m/s, 12.6 m/s, 13.6 m/s, 14.6 m/s, 15.6 m/s, and 16.6 m/s. The corresponding relation between the fluid velocity and the turbulence intensity is obtained, as shown in Table 2.

4. CFD Model Verification

In order to verify the accuracy of the CFD model, the experimental measurements of flow velocity and mass flow rate were taken before and after air went through the inlet

Figure 9: Experimental measurement.

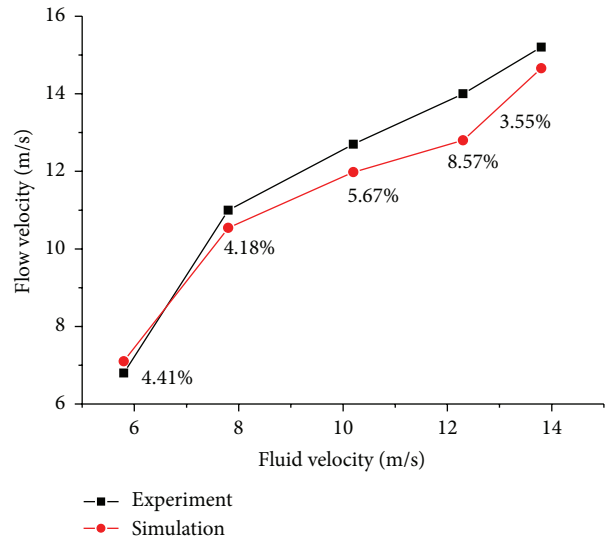

Figure 10: Relative error of the flow velocity between simulation and experiment in section.

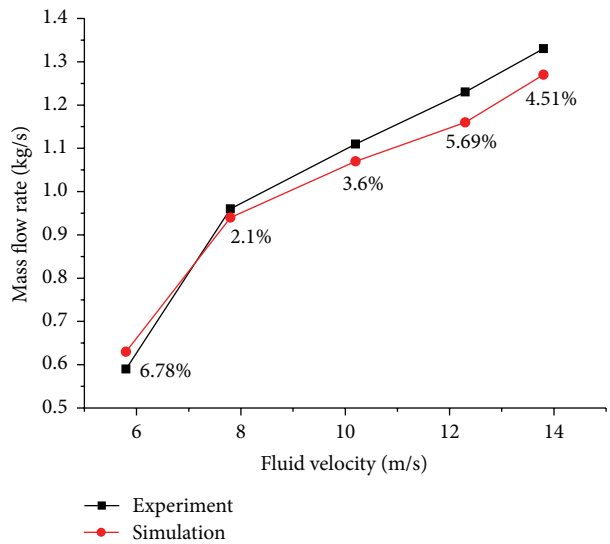

Figure 11: Relative error of the mass flow rate between simulation and experiment in section.

grid in the engine compartment of practical vehicles. In the test, the environmental atmospheric pressure was 100 kPa, and the temperature was 24°C. Six measure points were arranged 10 mm away from the grid wall and the engine operations were set with different speeds. Wind speed measuring instrument was employed to get the air mean flow velocity and mean mass flow rate under different speeds and different measurement points (Figure 9). Furthermore, the results were taken as the measure parameters of the section 10 mm away from the grid wall and the mean flow velocities before air went through the inlet grid were set as the inlet boundary in virtual wind model. Then numerical simulation was presented. Finally, the relative error between the measure parameter values after air went through the inlet grid calculated by numerical simulation and the experimental values can be obtained, as shown in Figures 10 and 11. And the formula of relative error is defined by

$$\mathrm{Re} = \left| \frac{y_{\text{experiment}} - y_{\text{simulation}}}{y_{\text{experiment}}} \right| \times 100\%. \quad (7)$$

According to the comparison, the relative errors of simulation and experiment are within 9%, which mainly resulted from the accuracy of the turbulence model, the simplification of simulation model, and the test precision of experiment [28]. In general, the results of numerical simulation and experimental test have a good consistency. Therefore, the established CFD model is verified to be accurate.

5. Result of Numerical Simulation

The modules of energy and acoustics in Fluent were applied and the numerical simulation was done. Based on the requirement of iteration, the calculation was decided to converge if the residual values of physical variable achieved the convergence criteria.

The THR in the inlet and outlet of virtual wind tunnel was taken as the indicator to evaluate heat dispersion and the ASPL of grid wall was taken as the indicator to evaluate aerodynamic noise. And then the effects of different grid forms and different porosities on the flow field, temperature field, and sound field of the CFD model were researched.

5.1. Calculation Result of Flow Field. After the engine compartment works for some time, the inner capsule can reach a thermal balancing state, which means the heat generated by components is almost equal to its emission. At this point, the temperature field inside the engine compartment has been in a stable condition. Due to the space limitations, here the temperature field distributions of airflow are only given at the fluid velocity of 16.6 m/s under three grid forms (Figures 12, 13, and 14), as well as the velocity vector distributions (Figures 15, 16, and 17).

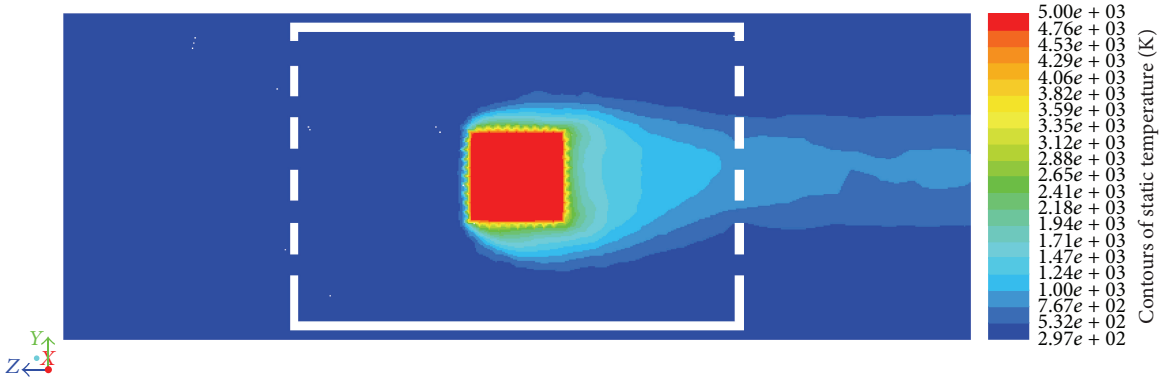

Figure 12: Temperature field distribution of the round hole in the section $X = 0$.

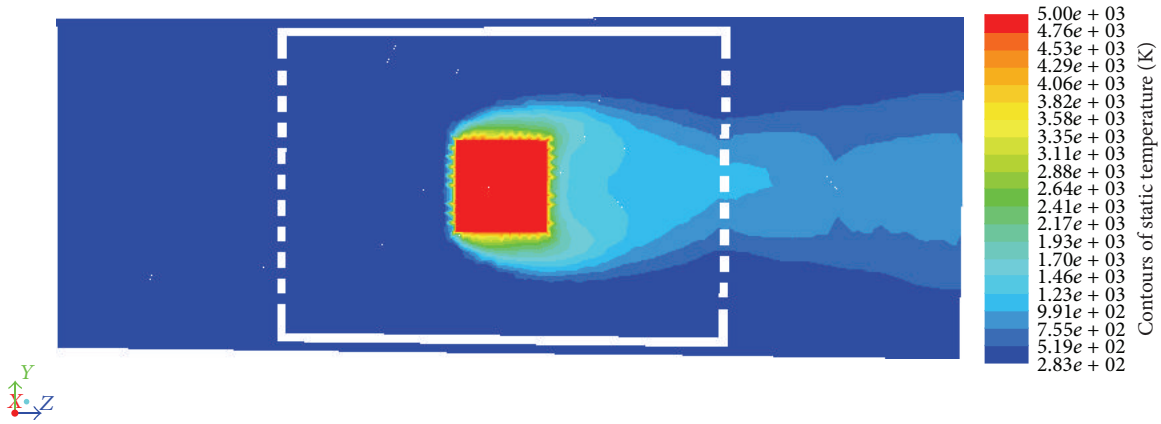

Figure 13: Temperature field distribution of the long hole in the section $X = 0$.

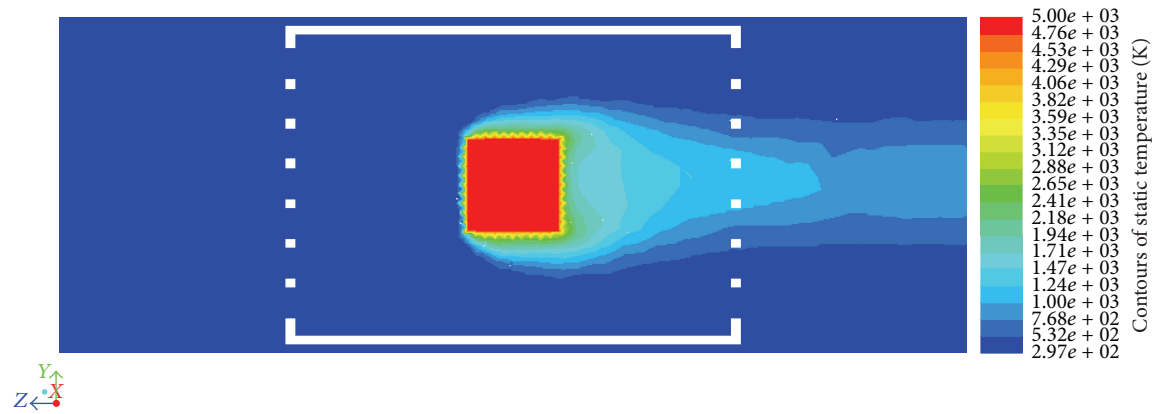

Figure 14: Temperature field distribution of the square hole in the section $X = 0$.

From Figures 12, 13, and 14, it can be seen that the inner temperature of virtual wind tunnel under three grid forms presents to be gradient distribution. After air passes through heat source, its temperature declines gradually from the left to the right. It is mainly because air takes away heat along its flow direction and the heat makes exchange with surroundings when propagating.

Figures 15, 16, and 17 show that airflow movement remains relatively stable after air goes through grid from its inlet at first. When air touches the grids, the movement velocity of airflow increases rapidly and presents different velocity field distributions under different grid forms. The velocity distribution of the round hole is relatively decentralized, while the square hole's is relatively concentrated. It is mainly

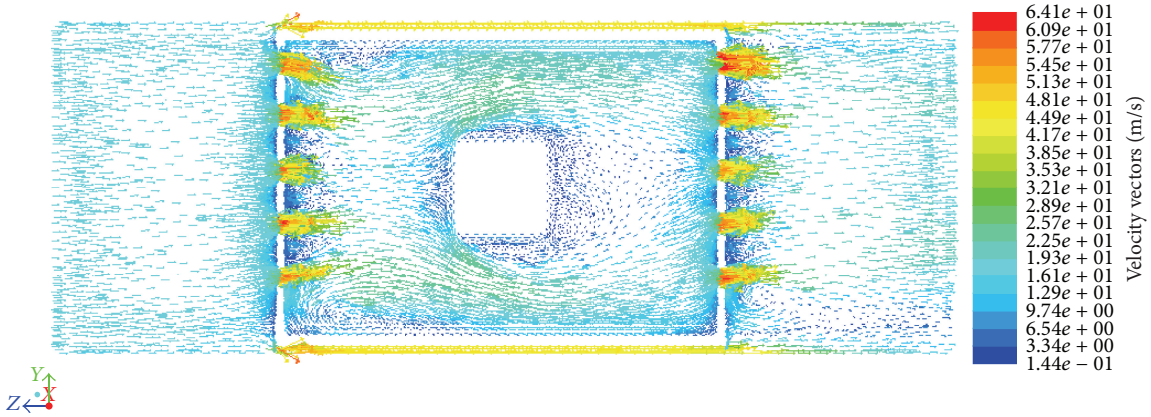

Figure 15: Velocity vector distribution of the round hole in the section $Z = 0$.

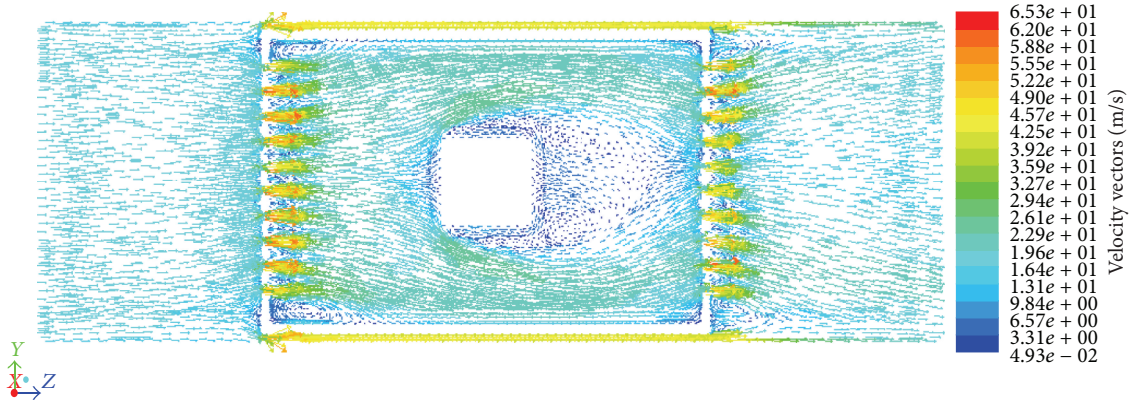

Figure 16: Velocity vector distribution of the long hole in the section $Z = 0$.

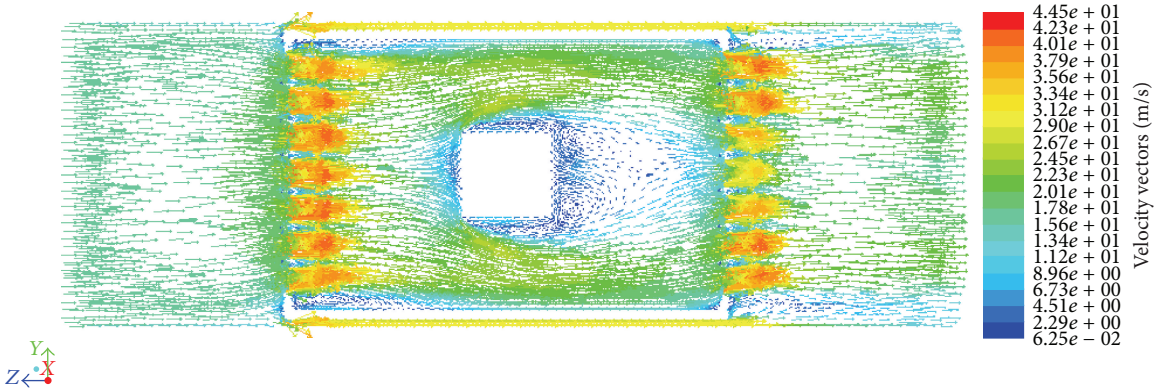

Figure 17: Velocity vector distribution of the square hole in the section $Z = 0$.

because the round hole amount in the longitudinal section is least under the same porosity and the space between round holes is the biggest. Therefore, the average airflow velocity through round holes decreases fast. In addition, due to facts that the space between square holes in the longitudinal section is the smallest and the side length of the square hole is the biggest, the average airflow velocity through square holes thus decreases slowly.

5.2. Calculation Result of THR. According to the Reports-Fluxes of Fluent software, the THR in the inlet and outlet of virtual wind tunnel can be easily obtained. Therefore, the relationship between the fluid velocity under three types of grid and the THR can be obtained (Figure 18).

From Figure 18, it can be found that the THR of the round hole grid in the virtual wind tunnel is the highest, and the square hole grid is next, while the long hole grid is the lowest.

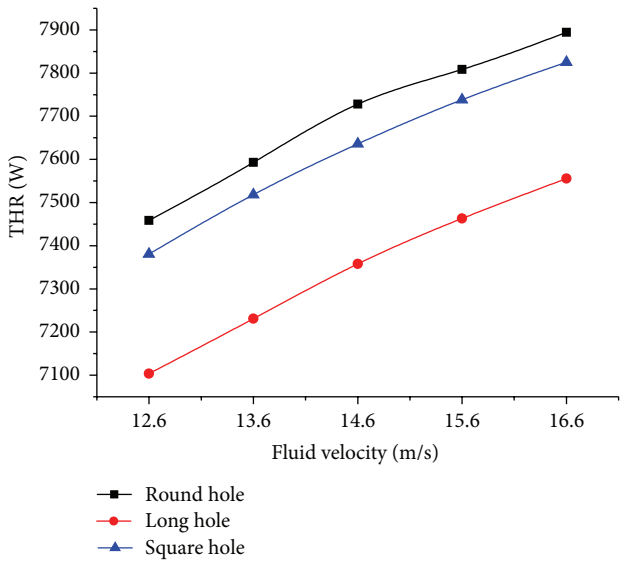

Figure 18: Relationship between fluid velocity and THR.

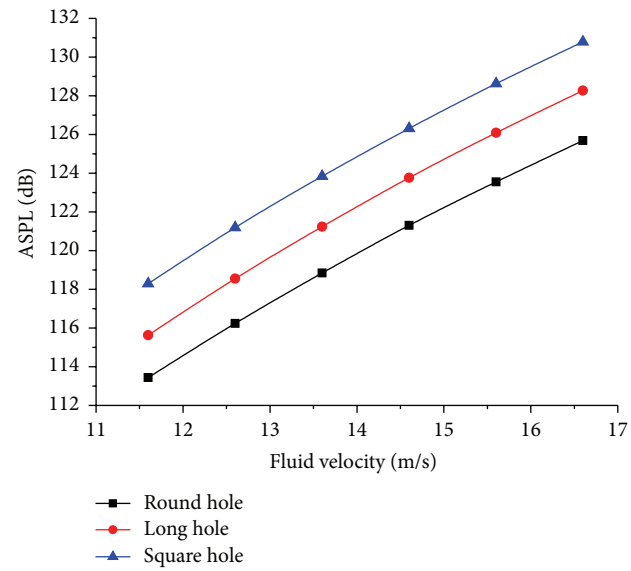

Figure 19: Relationship between the fluid velocity and ASPL in three grid forms.

There is the main reason that the grid structure form directly relates to resistance properties of airflow. In other words, it shows that the pressure drop when fluid passes through the round grids is obviously lower than that passing through the square grids. Furthermore, when fluid velocity increases constantly, the THR in the inlet and outlet of virtual wind tunnel under three types of grid nearly presents linear growth. It is because the bigger the fluid velocity is, the more the heat that can be taken away from the heat source is, which corresponds to the physical truth.

5.3. Calculation Result of ASPL. Based on the analysis of numerical simulation with the porosity to be 0.345, the variation rules between the ASPL generated in the grid wall and the fluid velocity are obtained when airflow passes through different grid forms, which is shown in Figure 19.

Figure 19 presents that the ASPL of simulation model when fluid passes through different grid forms has the same change tendency with fluid velocity under the same porosity, and it increases as fluid velocity increases. This is in accordance with the famous theory of Lighthill 8 power law on jet noise [29]. In addition, it can be seen that the ASPL is the highest when airflow passes through the square hole, while it is the lowest when through the round grid, which indicates that the aerodynamic noise is the lowest when airflow passes through the round hole grids.

5.4. Calculation Result of Porosity. From the analysis above, it can be easily concluded that the round hole grids should be adopted under the same porosity. Now research the change rules between the fluid velocity through the round hole grids under different porosities and the ASPL. The porosity is selected as 0.345, 0.4, 0.455, 0.51, and 0.565, and the corresponding diameter of the round hole can be calculated as 6 mm, 6.459 mm, 6.889 mm, 7.293 mm, and 7.677 mm, and the fluid velocity also is selected as 11.6 m/s, 12.6 m/s, 13.6 m/s, 14.6 m/s, 15.6 m/s, and 16.6 m/s. The relationship between the fluid velocity and the ASPL is calculated by the numerical simulation gained (Figure 20).

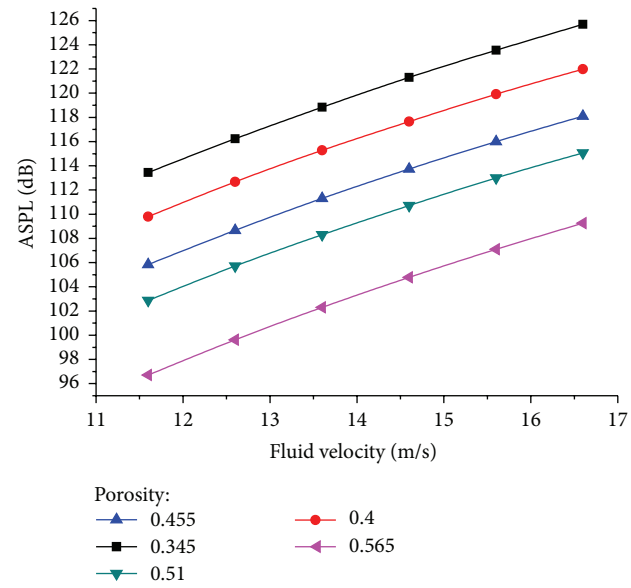

Figure 20: Relationship between the fluid velocity and the ASPL in different porosities.

Figure 20 demonstrates that the ASPL in the round grid wall increases as fluid velocity increases, which is in line with the actual situation. In addition, under the same fluid velocity, the larger the porosity is, the smaller the ASPL is. It is because of the different disturbance degrees under different contact areas; the bigger the diameter of the round hole is, the more stable the airflow movement is and the smaller the disturbance degree is.

6. Conclusions

(1) Based on the CFD method, the thermal-field and sound-field coupling model under different grid forms is established, which has the relatively high accuracy verified with the experiment. Through numerical simulation operated with energy equation and the FW-H equation of aeroacoustics, it makes a comprehensive study on the heat dispersion and aerodynamic noise of the round hole grid, long hole grid, and square hole grid, and thus the variation rules of flow field, thermal field, and sound field are obtained.

(2) Taking evaluation indicators of the THL in the inlet and outlet of virtual wind tunnel as well as the ASPL in the grid wall of simulation model, the heat dispersion and aerodynamic noise of three grid forms are studied. As the results show, under the same porosity, the round hole grid has the highest heat dispersion and airflow through the round hole and has the best resistance property, and the round hole grid has the lowest ASPL and its airflow has the smallest disturbance.

(3) Results show that the round hole is the best chosen in terms of grid form. And the bigger the porosity is, the smaller the ASPL in the grid wall is and the airflow is more stable. The numerical analysis results can provide a guidance for improving heat balance and reducing radiation noise in the engine compartment and hence reach the expected requirement of energy saving and noise reduction.

(4) The research on the coupled issue of thermal field and sound field under different grid forms has already been completed by theoretical analysis and numerical calculation. In addition, synthetically considering other grid structure forms and porosities to look for a better solution to energy saving and noise reduction and manufacturing the corresponding products to experimentally validate numerical simulation results are the future research direction.

Conflict of Interests

The authors declare that there is no conflict of interests regarding the publication of this paper.

Acknowledgments

This work was supported by the National Key Technologies R&D Program of China (no. 2013BAF07B04) and the Collaborative Innovation Center of High-End Equipment Manufacturing in Fujian.

References

[1] H. J. Cao, F. Liu, and Y. He, "Integrated task-assigning model of energy saving and noise reduction in the machining systems and its application," *Chinese Journal of Mechanical Engineering*, vol. 42, no. 5, pp. 97–102, 2006.

[2] Y. He and F. Liu, "Methods for integrating energy consumption and environmental impact considerations into the production operation of machining processes," *Chinese Journal of Mechanical Engineering*, vol. 23, no. 4, pp. 428–435, 2010.

[3] P.-P. Wang, C. Zhou, Y. Song, Y.-H. Zhang, and Z.-Y. Zhao, "A numerical study of effects on detection height of a radio acoustic sounding system influenced by atmospheric wind and temperature," *Acta Physica Sinica*, vol. 64, no. 10, Article ID 100205, 2015.

[4] L. Henriksson, P. Gullberg, E. Dahl, and L. Lofdahl, "CFD simulations of one period of a louvered fin where the airflow is inclined relative to the heat exchanger," *SAE International Journal of Engines*, vol. 8, no. 4, pp. 1733–1742, 2015.

[5] F. Wang, S.-C. Qin, and K.-L. Zhao, "Numerical simulation study on wheel loader tube-fin radiator air flow and heat transfer character," *Journal of Jilin University (Engineering and Technology Edition)*, vol. 39, supplement 1, pp. 196–199, 2009.

[6] P. Setlur, J. R. Wagner, D. M. Dawson, and E. Marotta, "An advanced engine thermal management system: nonlinear control and test," *IEEE/ASME Transactions on Mechatronics*, vol. 10, no. 2, pp. 210–220, 2005.

[7] Y.-L. Xu, Y.-B. Yang, B.-F. Zu, Q. Wang, D.-S. Li, and Y.-K. Cong, "Optimizing calculation and experimental research of intake port of automobile diesel engine," *Chinese Internal Combustion Engine Engineering*, vol. 34, supplement 1, pp. 65–71, 2013.

[8] M. Khaled, A. Alshaer, F. Hachem, F. Harambat, and H. Peerhossaini, "Effects of ground vehicle inclination on underhood compartment cooling," *International Journal of Automotive Technology*, vol. 13, no. 6, pp. 895–904, 2012.

[9] I. Bayraktar, "Computational simulation methods for vehicle thermal management," *Applied Thermal Engineering*, vol. 36, no. 1, pp. 325–329, 2012.

[10] T. Defraeye, B. Blocken, E. Koninckx, P. Hespel, and J. Carmeliet, "Aerodynamic study of different cyclist positions: CFD analysis and full-scale wind-tunnel tests," *Journal of Biomechanics*, vol. 43, no. 7, pp. 1262–1268, 2010.

[11] M. Schifko, H. Steiner, D. Fellhofer, X. Song, K. Verma, and C. Bauinger, "Transient dip paint simulation of entire car bodies within one day," *SAE International Journal of Materials and Manufacturing*, vol. 8, no. 2, pp. 523–533, 2015.

[12] N. Gil-Negrete, A. Rivas, and J. Viñolas, "Predicting the dynamic behaviour of hydrobushings," *Shock and Vibration*, vol. 12, no. 2, pp. 91–107, 2005.

[13] J. O. Aguilar, J. Xaman, G. Álvarez, I. Hernández-Pérez, and C. López-Mata, "Thermal performance of a double pane window using glazing available on the Mexican market," *Renewable Energy*, vol. 81, pp. 785–794, 2015.

[14] X. Cui, K. J. Chua, and W. M. Yang, "Numerical simulation of a novel energy-efficient dew-point evaporative air cooler," *Applied Energy*, vol. 136, pp. 979–988, 2014.

[15] I. C. Tolias, A. G. Venetsanos, N. Markatos, and C. T. Kiranoudis, "CFD modeling of hydrogen deflagration in a tunnel," *International Journal of Hydrogen Energy*, vol. 39, no. 35, pp. 20538–20546, 2014.

[16] A. F. Pouangué, M. Sanjosé, S. Moreau, G. Daviller, and H. Deniau, "Subsonic jet noise simulations using both structured and unstructured grids," *AIAA Journal*, vol. 53, no. 1, pp. 55–69, 2015.

[17] N. Sinha and J. P. Erwin, "Prediction of jet noise for realistic flow problems using large eddy simulation," *International Journal of Aeroacoustics*, vol. 11, no. 7-8, pp. 851–884, 2012.

[18] H. Xia, "Turbulent jet characteristics for axisymmetric and serrated nozzles," *Computers and Fluids*, vol. 110, no. 1, pp. 189–197, 2015.

[19] C. Bogey, C. Bailly, and D. Juvé, "Noise investigation of a high subsonic, moderate reynolds number jet using a compressible large eddy simulation," *Theoretical and Computational Fluid Dynamics*, vol. 16, no. 4, pp. 273–297, 2003.

[20] M. J. Fisher, G. A. Preston, and C. J. Mead, "A modelling of the noise from simple coaxial jets, part II: with heated primary flow," *Journal of Sound and Vibration*, vol. 209, no. 3, pp. 405–417, 1998.

[21] J. E. F. Williams and D. L. Hawkings, "Sound generation by turbulence and surfaces in arbitrary motion," *Philosophical Transactions of the Royal Society*, vol. 264, no. 1151, pp. 321–342, 1969.

[22] Z. Nitzkorski and K. Mahesh, "A dynamic end cap technique for sound computation using the Ffowcs Williams and Hawkings equations," *Physics of Fluids*, vol. 26, no. 11, Article ID 115101, 2014.

[23] Z.-H. Han, W.-P. Song, and Z.-D. Qiao, "Aeroacoustic calculation for helicopter rotor in hover and in forward flight based on FW-H equation," *Acta Aeronautica et Astronautica Sinica*, vol. 24, no. 5, pp. 400–404, 2003.

[24] V. B. Nguyen, H. J. Poh, and Y.-W. Zhang, "Predicting shot peening coverage using multiphase computational fluid dynamics simulations," *Powder Technology*, vol. 256, pp. 100–112, 2014.

[25] H. Li, Y. Li, F. Gao, Z. Zhao, and L. Xu, "CFD-DEM simulation of material motion in air-and-screen cleaning device," *Computers and Electronics in Agriculture*, vol. 88, pp. 111–119, 2012.

[26] Y. H. Yu, S. H. Park, C.-J. Kim, S. Sung, and K. H. Jin, "Noise and energy conservation," *Journal of the Korean Physical Society*, vol. 53, no. 4, pp. 1919–1922, 2008.

[27] G. N. Xie, J. Liu, W. H. Zhang, G. Lorenzini, and C. Biserni, "Numerical prediction of flow structure and heat transfer in square channels with dimples combined with secondary half-size dimples/protrusions," *Numerical Heat Transfer Part A: Applications*, vol. 65, no. 4, pp. 327–356, 2014.

[28] G. Y. Ma, L. M. Du, and M. Z. Xie, "On new eddy viscosity models of turbulent flow in the cylinder of internal combustion engine," *Transactions of CSICE*, vol. 20, no. 5, pp. 433–443, 2002.

[29] K. Viswanathan, "Mechanisms of jet noise generation: classical theories and recent developments," *International Journal of Aeroacoustics*, vol. 8, no. 4, pp. 355–407, 2009.